Tailoring Unique Mesopores of Hierarchically Porous Structures for Fast Direct Electrochemistry in Microbial Fuel Cells

*Long Zou, Yan Qiao, Zhen-Yu Wu, Xiao-Shuai Wu, Jia-Le Xie, Shu-Hong Yu, Jinhong Guo, and Chang Ming Li**

With the ever-growing shortage of traditional fossil fuels and worsening environmental pollution, microbial fuel cell (MFC) as an extraordinary green energy technology has fueled substantial research interest due to its room temperature operation, low expense, zero pollution, and waste-treatment capability.[1–3] However, the low power density of MFC mainly resulting from the sluggish bacterial extracellular electron transfer between microbe and electrode limits its practical applications.[3–6] An MFC anode involves both bio- and electro-catalytic process.[2,7] Extensive studies have been devoted to exploring macroporous anode materials from both macroscopical porous scaffold (nickel foam, sponge, textile, cardboard, etc.)[7,8] and natural biomass materials (pomelo peels, kenaf, loofah, etc.)[9] to improve bacterial cells (biocatalysts) loading while promoting the direct electron transfer via the bacterial out membrane *c*-type cytochromes and/or the conductive pili (bacterial nanowires)[5,6] for high MFC performance; nevertheless, the power density is still much lower than the conventional fuel cells, and that obviously is due to the slow electron transfer through the nonconductive or poorly conductive microbes biocatalysts.[7–9] Thus, except increasing the loading of the biocatalys, it is also essential to tailor a unique nanopore structure for enhancement of the direct electrochemistry process between microbes and electrode. It has been noted that for many electricigens such as *Shewanella* spp. the electron transfer mediated by endogenously generated electron shuttles shows equal or even more important role in MFC than that through membrane, and both have been recognized as a direct electrochemistry pathway because there is no need for introducing additional electron mediators.[2,10–13] Nanoporous activated carbon with high surface area has been proven to offer better *Shewanella oneidensis* anode performance than using some plane electrodes such as carbon felt, which is attributed to the enhanced electron transfer mediated by the self-secreted flavins[5,14] but the effect mechanism of the porous structure on the direct electrochemistry has not been disclosed yet. Further, it has been suggested that a rationally tailored hierarchically porous anode with pore sizes <10 nm is important for the electrocatalytic process [7,15] when using the macropores to grow high loading of microbes for a high performance MFC but there is no direct evidence to show the meso- (2–10 nm) and micro- (<2 nm) pore structure effects on the direct electrochemistry, respectively.

Carbon fiber materials have been used as anodes for improvement MFC performances.[16] Herein, a better hierarchically porous carbon nanofiber (CNF) aerogel is prepared from bacterial cellulose (BC) produced by a microbial fermentation process in an industrial scale [17] and further used to for MFC anodes. The BC pellicles have been reported as an excellent precursor for producing a 3D macroporous architecture through a facile carbonization process.[18,19] Due to its excellent conductivity, high biocompatibility, low cost, and large amount of macropores, the CNF aerogel material is expected to promote electroactive biofilm growth for MFC anodes. In addition, since the substantially enhancement mechanism of nanopore structure of the carbon nanofibers on improving MFC performance is still a mystery, it is systematically investigated with tailoring the nanopore structure by different pyrolytic temperatures for the first time.

To fabricate CNF aerogels, the purified BC pellicles were cut into rectangular slices and then freeze-dried to form bacterial cellulose aerogels,[19] followed by pyrolysis at 600–1100 °C under argon atmosphere. Scanning electron microscopy (SEM) images (**Figure 1**a,b and Figure S1, Supporting Information) show that all obtained monolithic CNF aerogels after the pyrolysis treatment can maintain the original 3D porous interconnected network structure of the bacterial cellulose aerogels without obvious difference except the much rougher

L. Zou, Dr. Y. Qiao, X.-S. Wu, Dr. J.-L. Xie, Prof. C. M. Li
Institute for Clean Energy and Advanced Materials
Southwest University
Chongqing 400715, China
E-mail: ecmli@swu.edu.cn
L. Zou, Dr. Y. Qiao, X.-S. Wu, Dr. J.-L. Xie, Prof. C. M. Li
Faculty of Materials and Energy
Southwest University
Chongqing 400715, China
L. Zou, Dr. Y. Qiao, X.-S. Wu, Dr. J.-L. Xie, Prof. C. M. Li
Chongqing Key Laboratory for Advanced Materials and Technologies of Clean Energies
Chongqing 400715, China
Z.-Y. Wu, Prof. S.-H. Yu
Department of Chemistry
Division of Nanomaterials and Chemistry
Hefei National Laboratory for Physical Science at Microscale
University of Science and Technology of China
Hefei, Anhui 230026, China
Dr. J. Guo, Prof. C. M. Li
Institute of Materials Science and Devices
Suzhou University of Science and Technology
Suzhou 215011, China

DOI: 10.1002/aenm.201501535

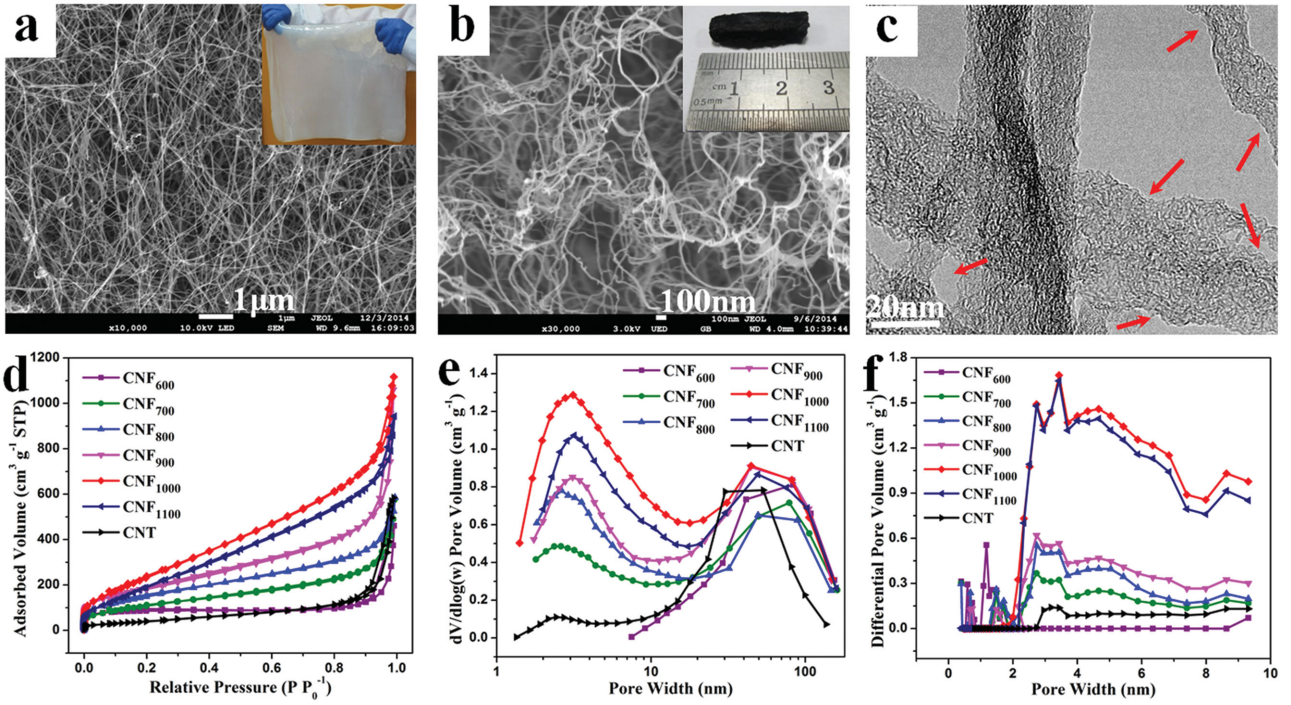

Figure 1. a) SEM images of BC aerogel (inset: the photograph of BC pellicle) and b) CNF aerogel after high-temperature pyrolysis (inset: the photograph of CNF aerogel). c) TEM image of CNF aerogel. d) Nitrogen adsorption–desorption isotherms, e) BJH pore size distributions, and f) DFT pore size distribution (<10 nm) of CNF aerogels prepared at different pyrolytic temperatures.

inner surface than its outside surface due to the pressing process in preparation of the original BC pellicles (see Figure S2 in the Supporting Information). The as-prepared CNF aerogels slabs were pulverized into powders for exposing more inner macropores for bacterial growth, and then were ready to be coated on conventional carbon cloths as anodes. Transmission electron microscopy (TEM) images (Figure 1c and Figure S3, Supporting Information) display that the CNF with a diameter of 10–30 nm are highly interconnected with many junctions to form networked macropores. X-ray diffraction (XRD) patterns (see Figure S4 in the Supporting Information) illustrate that the CNF mainly comprises randomly orientated graphitic layers.[19] Fourier transformed infrared (FTIR) spectra (see Figure S5 in the Supporting Information) reveal that the main absorption peaks of oxygen-containing functional groups in BC aerogels gradually weaken and disappear with the increased pyrolytic temperature.[19]

Surface area and pore structure of an electrode material, which could be greatly affected by the pyrolytic temperature, play a crucial role in electrocatalytic performance.[2,15,20] The Brunauer–Emmett–Teller (BET) surface areas and pore size distributions of CNF aerogels pyrolyzed at different temperatures were examined by nitrogen adsorption–desorption isotherm measurement (Figure 1d), showing that the BET surface area increases rapidly from 268.42 to 964.79 $m^2 g^{-1}$ over the pyrolytic temperature of 600–1000 °C but falls slightly to 845.68 $m^2 g^{-1}$ at 1100 °C (see Table S1 in the Supporting Information). The BET surface area of CNF_{1000} aerogel is much larger than that of carbon nanotubes (CNTs) by about sixfold more. The plots of pore size distribution based on Barrett–Joyner–Halenda (BJH) model (Figure 1e) indicate that all of the CNF aerogels have a wide ranging of macropores with an average pore size near 50 nm resulting from stacked carbon nanofibers network. Interestingly, the pyrolytic temperature has significant impact on tuning nanopores (<10 nm) of CNF aerogels as shown in the plots of pore size distribution based on density functional theory (DFT) model (Figure 1f), which is good for analysis of distributions of micropores and mesopores in a porous material.[21] The CNF_{600} aerogel only has a large amount of micropores (<2 nm); with increasing the pyrolytic temperature, the micropores gradually disappear but mesopores (2–10 nm) grow. When the pyrolytic temperature reaches to 1000 °C, all micropores almost disappear and abundant mesopores are generated along with the increased average pore size, which could be ascribed to the consecutive emission of many non-carbons and carbon-containing components for eliminating the micropores during the pyrolysis.[22] These mesopores can be observed in the high-resolution TEM image (Figure 1c). In addition, the BET surface areas of CNF aerogels are proportional to their pore volume, indicating that the enlarging surface area after pyrolysis treatment is mainly attributed to the transformation from micropores to the abundant mesopores.

The effect of surface area and nanopore structure of CNF aerogels on the direct electrochemistry of endogenous flavin mediators was investigated by cyclic voltammetry (CV) and electrochemical impedance analysis (EIS) in a three-electrode electrochemical cell (EC) filled with anaerobic *Shewanella putrefaciens* CN32 cell suspension. Meanwhile, CNT, a frequently used nanocarbon material, whose morphology is very similar to CNFs, and carbon cloth are chosen for comparisons. Except for

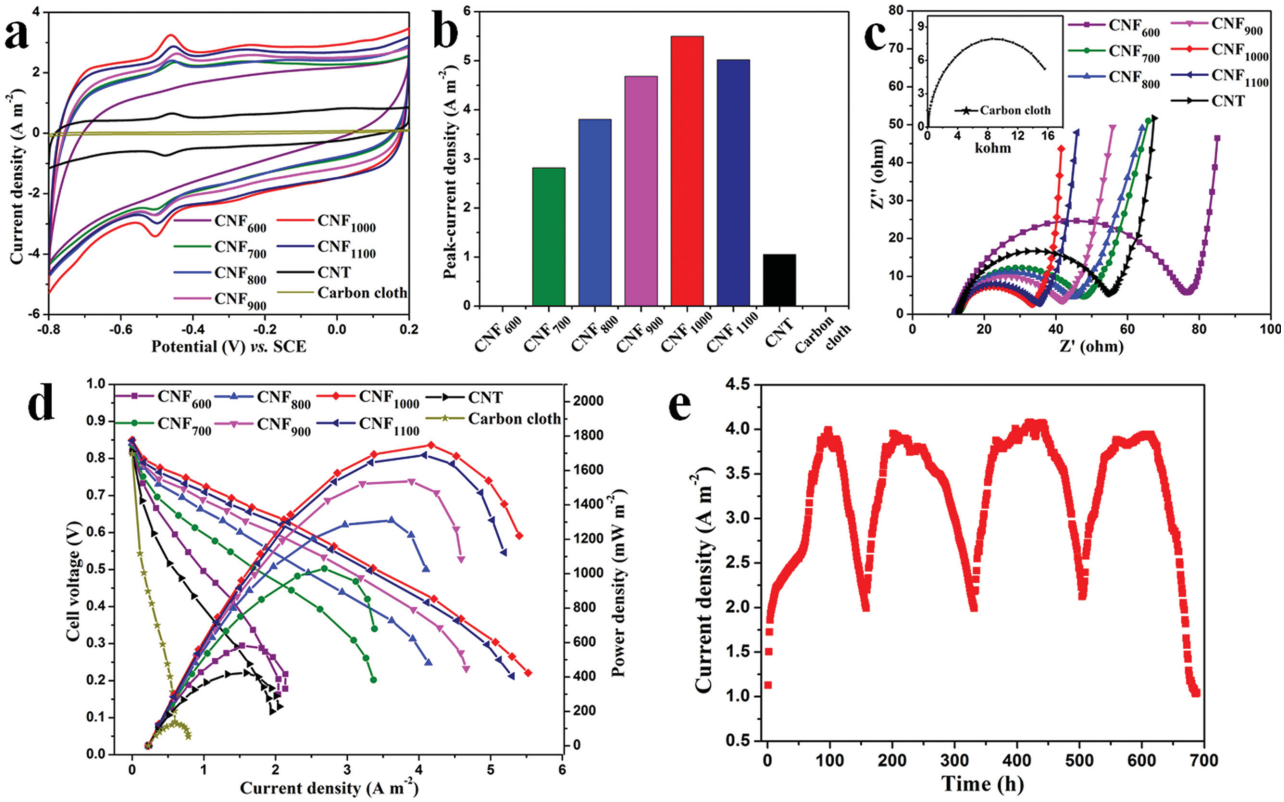

Figure 2. a) Cyclic voltammograms at a scan speed of 10 mV s^{-1}, b) corresponding oxidation peak-current density around –0.45 V, and c) Nyquist plots of different anodes in three-electrode electrochemical cells. d) Polarization and output power density plots of different anodes in dual-chamber MFCs; e) four-cycle discharge plot of CNF_{1000} anode-based dual-chamber MFC with an external loading resistance of 1000 Ω.

CNF_{600} anode and carbon cloth anode, CV curves (**Figure 2**a) of CNFs and CNT anodes show a well-defined redox pair around –0.45 V (vs saturated calomel electrode, SCE), which could be ascribed to the direct electrochemistry behavior of *S. putrefaciens* CN32 cells because no exogenous electron shuttle is added into the electrolyte. The endogenous-secreted flavins from *S. putrefaciens* CN32 cells have been reported to initiate the direct electrochemistry.[6,23] In addition, there is another wide but weak redox pair centered at about –0.3 V, which is more clearly observed in the background-subtracted CV (see Figure S6 in the Supporting Information), suggesting being the direct electron transfer through out membrane *c*-type cytochromes of *S. putrefaciens* CN32 biofilm.[6,23] Obviously, the direct electrochemistry from the membrane-base one is much poorer than the endogenous flavins since it takes much longer time to reach the diffusion-controlled peak current and the peak potential is more positive, indicating the former has more sluggish reaction rate and lower electrocatalytic activity. The calculated charge capacity, representing the electroactive surface area,[24] of CNF aerogels pyrolyzed at different temperatures increase with the measured BET surface area. In contrast, no identical redox pair at –0.45 V is observed in the CV of CNF_{600} anode and carbon cloth, indicating undetected direct electrochemistry of flavin mediators on these electrodes. However, with converting the micropores to mesopores after pyrolysis, the prominent anodic oxidation peak around –0.45 V occurs, and the peak current density increases with the increased volume of mesopores in the CNF aerogels (Figure 1f and Figure 2b). For the CNT control anode, its anodic oxidation peak current density is much smaller than that of CNF_{1000} anode due to its much less mesopore volume. In addition, the Nyquist plots (Figure 2c) show that the CNF_{1000} anode exhibits the lowest charge transfer resistance (R_{ct}) of about 21.50 Ω, which is consistent with the CV results. It can be concluded that the mesopores indeed enhanced the charge transfer rate of the direct electrochemistry.

The enhancement mechanism of mesopores can be well-explained. Notably, the sizes of the two main flavin mediators, riboflavin and flavin mononucleotide, secreted from *Shewanella* spp.[6,10,12] are about 1–1.5 nm at the lowest energy state (see Figure S7 in the Supporting Information). It is also reported that the electron transfer mediated by flavins is executed at 1,5-nitrogens via a two-electron reaction between their quinone and hydroquinone species.[25] It is very hard to have the two-electron passway happening on a flat surface since the two 1,5-nitrogen atoms are separated by two carbon atoms and are not able to be absorbed simultaneously due to steric effect. Further, the micropores have sizes smaller than or barely same as that of flavins, not allowing their easy diffusion into the pore surface for surface absorption. It is known that bioxygen molecules in a simultaneous bridge-adsorption mode can achieve the most efficient four-electron transfer passway[26] but it needs a matched steric nanostructure for such an adsorption such as a cylindrical dicobalt face-to-face porphyrin-modified electrode surface for the bimolecule bridge adsorption.[27] Thus, it is

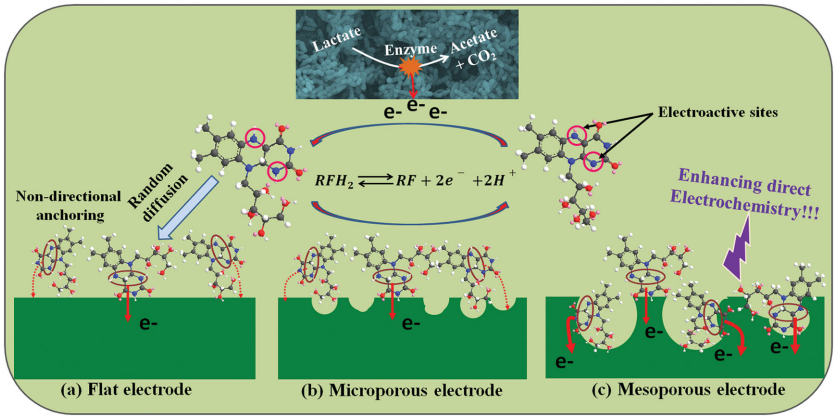

Figure 3. Schematic illustration of the enhancement mechanism of mesopore structure for the direct electrochemistry of flavins. The two-electron redox reaction between flavins' quinone and hydroquinone species is executed at 1,5-nitrogens, which are separated by two carbon atoms so that, a) it is very hard to have two-electron redox happening on a flat surface due to a strong steric-hindrance effect. b) The micropores have sizes comparable with that of flavins not allowing their diffusion into the pore surface. c) Whereas the mesopores offer large enough 3D pores behaving like "bags" to trap the flavins and their curvature or kink surface could offer more opportunities for directly contacting the two electroactive sites and thus promoting the two-electron transfer direct electrochemistry.

also very critical to offer a steric nanostructure to match and simultaneously adsorb the two reaction sites of flavin for its direct electrochemistry. According to our results, a reasonable mesopore-enhancement mechanism for direct electrochemistry is proposed as shown in **Figure 3**, in which on a flat electrode such as carbon cloth or porous electrode without mesopores such as CNF_{600} the two electroactive sites of the flavins are very hard to simultaneously access to or being absorbed on the electrode surface for the fast direct two-electron transfer passway due to a strong steric-hindrance effect. That is possible because the CNF_{600} anode and carbon cloth exhibit indiscernible direct electrochemistry of flavins (Figure 2a). For a porous electrode with abundant mesopores such as CNF_{1000}, the mesopores can not only further enlarge the surface area of the electrode, but more importantly also provide large enough 3D pores for flavins to move in and out. The 3D mesopore behaves like a proper sizable "bag" to trap the flavin mediators and more importantly its curvature or kink surface could offer more opportunities to overcome the steric effect for directly contacting the two electroactive sites for effective surface absorption and to promote the two-electron transfer direct electrochemistry as exemplified in Figure 3c. This mechanism can be well supported by the direct electrochemistry results discussed above.

The bioelectrocatalytic performances of as-prepared CNF, CNT and carbon cloth anode were further investigated in batch-type dual-chamber MFCs. Figure 2d shows that the output power densities of CNF anodes prepared at different pyrolysis temperature are in good agreement with their direct electrochemical performances of flavins. In particular, the CNF_{1000} anode delivers a maximum power density of 1747 mW m^{-2} in the batch-type dual-chamber MFC, which is threefold higher than that of CNF_{600} anode (582 mW m^{-2}), further confirming that the enhancement effect of the mesopores on the direct electrochemistry in MFCs. Moreover, the output power density of the CNF_{1000} anode is around 4-fold and 14-fold higher than that of CNT anode (423 mW m^{-2}) and carbon cloth anode (127 mW m^{-2}), respectively. The discharge plot (Figure 2e) of CNF_{1000} anode with a constant load of 1000 Ω, which is equal to the internal resistance of MFC estimated from its polarization curve, shows a high plateau current density of about 3.9 A m^{-2} and a long discharge life for more than 150 h in each batch. When the output current drops due to the electron donor (lactate) depletion over time, replenishment of fresh lactate yields an immediate recovery of current, indicating that the CNF_{1000} anode has an excellent stability for long-time operation. After discharge, the surface morphologies of all anodes were examined by SEM; very large amounts of bacterial cells are adhered with each other to form a thick integrated biofilm on the CNF anodes (**Figure 4**a and Figure S8, Supporting Information). Moreover the bacterial cells grow into the inner large macropores of CNF

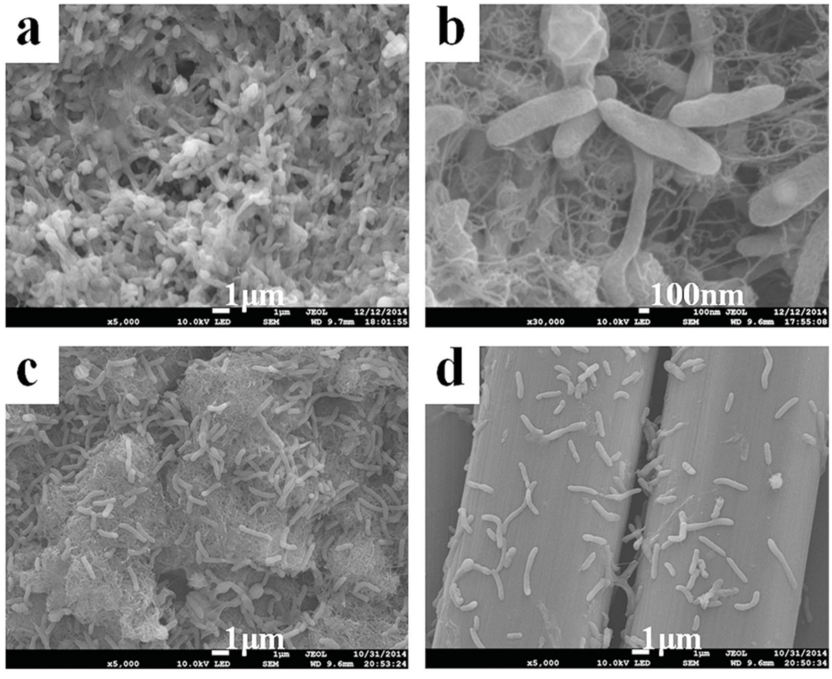

Figure 4. Comparison of biocompatibility of CNF aerogel with carbon CNT and carbon cloth. SEM images of bacteria cells grown on different anodes after one-cycle discharge: a,b) CNF, c) CNT, and d) carbon cloth.

aerogels (Figure 4b). This result indicates that CNF aerogels have a superior biocompatibility than CNT and carbon cloth (Figure 4c,d) as the CNF one is derived from naturally biosynthetic materials. The densely electroactive biofilm enables a large amount of loading of microbes, a biocatalyst to secrete more endogenous mediators[6] for the direct electrochemistry, which is an additional contribution to the enhanced power density over the mesopore contribution. The CNF_{1000} aerogel was also integrated into a nickel foam, a frequently used 3D macroporous, conductive metal scaffold[7] (pore size >10 μm), which delivers a maximum power density of 4601 mW m^{-2} and a plateau current density of about 6.5 A m^{-2} at a constant load of 800 Ω (Figure S9, Supporting Information), a value larger than that of graphene/nickel foam anode reported in previous work.[7] The hierarchically porous graphene/nickel foam anode also has a certain amount of mesopores[7] but less than that of CNF_{1000} aerogel. Apparently, the increased power density of CNF_{1000}@nickel foam anode should attributed to the increased mesopores. Therefore, tailoring a rational nanostructured electrode to possess both macropores and mesopores to promote both bio- and electro-catalytic processes is essential to greatly enhance the power density.

For a long time scientists are always concerned that the endogenous mediator-based direct electrochemistry may impede the practical industrial applications such as wastewater treatment or using liquid fuels since washing out of the fuel-exhausted electrolyte for replacement could flush the electron mediators away during continuous operation. Here, the potential of the CNF_{1000} anode for continuous-mode operation in a dual-chamber MFC is preliminarily evaluated through a simple replacement of the original discharging medium with fresh flavin-free medium during the plateau period of current generation. After replacement of the original medium, the current density generated by carbon cloth anode rapidly reduced to 20% (see Figure S10 in the Supporting Information), which is consistent with the reported works[10,13] and confirms the validity of this experiment method. Nevertheless, it is surprising that only 3% drop for CNF_{1000} anode is observed, and this negligible decrease can be rapidly reverted to 100% in a short time. We argue that the endogenous mediator-based direct electrochemistry should mainly account on the immediately self-secreted ones from the microbes rather than the accumulated mediators in the electrolyte during the discharge process. This work experimentally confirms that the endogenous electron mediator based direct electrochemistry can survive the wash-out procedure without decayed performance at least in this case for long term operation, thus holding great promise for such technology in practical industrial applications.

In summary, we fabricate a highly biocompatible hierarchically porous structure comprising macro-, meso- or micropores from cost-effective bacterial cellulose through a facile carbonization approach, and it is further tailored for its nanopore structure (<10 nm) by pyrolysis at different temperatures to systematically investigate the effect of nanostructure on the direct electrochemistry for the first time. Result shows that with increasing the pyrolytic temperature, the micropores gradually convert to mesopores until the former completely disappear, and most importantly discloses that the mesopore structure is necessary to have the direct electrochemistry of the endogenous flavin mediators and more converted mediators can produce stronger direct electrochemistry to greatly boost the anode power density in MFCs. The enhancement mechanism of mesopores on direct electrochemistry is attributed to their size and curvature, which can trap the mediator in and overcome the steric effect of the mediator allowing the two-electroactive sites simultaneously access the electrode surface for the direct two-electron transfer. Meanwhile, this hierarchically porous structure has enough macropores with high biocompatibility to grow microbe catalyst film extending into the inner pores for rendering larger reaction surface while producing more endogenous electron mediators for direct electrochemistry. Thus, we argue that this work not only discloses the fundamental insights of the flavin direct electrochemistry, but may also demonstrate a universal approach to greatly improve the direct electrochemistry process by tuning more detail nanostructures via both size and surface morphology for electroactive sites allowing the mediator accessing the electrode surface. This could have a universal significance.

Experimental Section

Experimental details are included in the Supporting Information.

Supporting Information

Supporting Information is available from the Wiley Online Library or from the author.

Acknowledgements

We gratefully acknowledge the financial support from National Program on Key Basic Research Project of China (973 Program under Contract No. 2013CB127804), the Fundamental Research Funds for the Central Universities (Grant Nos. XDJK2015B018 and XDJK2014D036), National Natural Science Foundation of China (Grant No. 31200102), Institute for Clean Energy & Advanced Materials, Southwest University, Chongqing, P.R. China, Chongqing Key Laboratory for Advanced Materials and Technologies of Clean Energies.

Received: July 31, 2015
Revised: November 3, 2015
Published online: December 7, 2015

[1] B. E. Logan, *Nat. Rev. Microbiol.* **2009**, *7*, 375.
[2] Y. Qiao, S.-J. Bao, C. M. Li, *Energy Environ. Sci.* **2010**, *3*, 544.
[3] B. E. Logan, K. Rabaey, *Science* **2012**, *337*, 686.
[4] F. Zhao, R. C. T. Slade, J. R. Varcoe, *Chem. Soc. Rev.* **2009**, *38*, 1926.
[5] A. P. Borole, G. Reguera, B. Ringeisen, Z.-W. Wang, Y. Feng, B. H. Kim, *Energy Environ. Sci.* **2011**, *4*, 4813.
[6] Y. Yang, M. Xu, J. Guo, G. Sun, *Proc. Biochem.* **2012**, *47*, 1707.
[7] Y. Qiao, X.-S. Wu, C.-X. Ma, H. He, C. M. Li, *Rsc Adv.* **2014**, *4*, 21788.
[8] a) Z. He, J. Liu, Y. Qiao, C. M. Li, T. T. Y. Tan, *Nano Lett.* **2012**, *12*, 4738; b) X. Xie, M. Ye, L. Hu, N. Liu, J. R. McDonough, W. Chen, H. N. Alshareef, C. S. Criddle, Y. Cui, *Energy Environ. Sci.* **2012**, *5*, 5265; c) X. Xie, G. Yu, N. Liu, Z. Bao, C. S. Criddle, Y. Cui, *Energy Environ. Sci.* **2012**, *5*, 6862; d) Y.-C. Yong, X.-C. Dong, M. B. Chan-Park, H. Song, P. Chen, *Acs Nano* **2012**, *6*, 2394; e) H. Wang, G. Wang,

Y. Ling, F. Qian, Y. Song, X. Lu, S. Chen, Y. Tong, Y. Li, *Nanoscale* **2013**, *5*, 10283; f) X. Xie, L. Hu, M. Pasta, G. F. Wells, D. Kong, C. S. Criddle, Y. Cui, *Nano Lett.* **2011**, *11*, 291; g) S. Chen, G. He, Q. Liu, F. Harnisch, Y. Zhou, Y. Chen, M. Hanif, S. Wang, X. Peng, H. Hou, U. Schroeder, *Energy Environ. Sci.* **2012**, *5*, 9769.

[9] a) S. Chen, G. He, X. Hu, M. Xie, S. Wang, D. Zeng, H. Hou, U. Schroeder, *ChemSusChem* **2012**, *5*, 1059; b) S. Chen, Q. Liu, G. He, Y. Zhou, M. Hanif, X. Peng, S. Wang, H. Hou, *J. Mater. Chem.* **2012**, *22*, 18609; c) Y. Yuan, S. Zhou, Y. Liu, J. Tang, *Environ. Sci. Technol.* **2013**, *47*, 14525.

[10] a) E. Marsili, D. B. Baron, I. D. Shikhare, D. Coursolle, J. A. Gralnick, D. R. Bond, *Proc. Natl. Acad. Sci. USA* **2008**, *105*, 3968; b) X. Jiang, J. Hu, L. A. Fitzgerald, J. C. Biffinger, P. Xie, B. R. Ringeisen, C. M. Lieber, *Proc. Natl. Acad. Sci. USA* **2010**, *107*, 16806.

[11] Y. Qiao, C. M. Li, S.-J. Bao, Z. Lu, Y. Hong, *Chem. Commun.* **2008**, *11*, 1290.

[12] E. D. Brutinel, J. A. Gralnick, *Appl. Microbiol. Biot.* **2012**, *93*, 41.

[13] a) A. Jain, X. Zhang, G. Pastorella, J. O. Connolly, N. Barry, R. Woolley, S. Krishnamurthy, E. Marsili, *Bioelectrochemistry* **2012**, *87*, 28; b) N. J. Kotloski, J. A. Gralnick, *Mbio* **2013**, *4*, e00553.

[14] a) E. Kipf, J. Koch, B. Geiger, J. Erben, K. Richter, J. Gescher, R. Zengerle, S. Kerzenmacher, *Bioresour. Technol.* **2013**, *146*, 386; b) E. Kipf, R. Zengerle, J. Gescher, S. Kerzenmacher, *ChemElectroChem* **2014**, *1*, 1849.

[15] C. M. A. Parlett, K. Wilson, A. F. Lee, *Chem. Soc. Rev.* **2013**, *42*, 3876.

[16] a) S. Chen, H. Hou, F. Harnisch, S. A. Patil, A. A. Carmona-Martinez, S. Agarwal, Y. Zhang, S. Sinha-Ray, A. L. Yarin, A. Greiner, U. Schroeder, *Energy Environ. Sci.* **2011**, *4*, 1417; b) S. S. Manickam, U. Karra, L. Huang, B. Nhu-Ngoc, B. Li, J. R. McCutcheon, *Carbon* **2013**, *53*, 19.

[17] a) M. Iguchi, S. Yamanaka, A. Budhiono, *J. Mater. Sci.* **2000**, *35*, 261; b) H. Yano, J. Sugiyama, A. N. Nakagaito, M. Nogi, T. Matsuura, M. Hikita, K. Handa, *Adv. Mater.* **2005**, *17*, 153.

[18] a) L.-F. Chen, Z.-H. Huang, H.-W. Liang, W.-T. Yao, Z.-Y. Yu, S.-H. Yu, *Energy Environ. Sci.* **2013**, *6*, 3331; b) L.-F. Chen, Z.-H. Huang, H.-W. Liang, H.-L. Gao, S.-H. Yu, *Adv. Funct. Mater.* **2014**, *24*, 5104; c) Z.-Y. Wu, H.-W. Liang, C. Li, B.-C. Hu, X.-X. Xu, Q. Wang, J.-F. Chen, S.-H. Yu, *Nano Res.* **2014**, *7*, 1861.

[19] Z.-Y. Wu, C. Li, H.-W. Liang, J.-F. Chen, S.-H. Yu, *Angew. Chem. Int. Ed.* **2013**, *52*, 2925.

[20] J. Zhang, C. M. Li, *Chem. Soc. Rev.* **2012**, *41*, 7016.

[21] J. Landers, G. Y. Gor, A. V. Neimark, *Colloid Surf. A* **2013**, *437*, 3.

[22] X. Yang, D. Wu, X. Chen, R. Fu, *J. Phys. Chem. C* **2010**, *114*, 8581

[23] D. Baron, E. LaBelle, D. Coursolle, J. A. Gralnick, D. R. Bond, *J. Biol. Chem.* **2009**, *284*, 28865.

[24] a) Y. Qiao, S.-J. Bao, C. M. Li, X.-Q. Cui, Z.-S. Lu, J. Guo, *Acs Nano* **2008**, *2*, 113; b) Y. Qiao, X.-S. Wu, C. M. Li, *J. Power Sources* **2014**, *266*, 226.

[25] D. E. Ross, J. M. Flynn, D. B. Baron, J. A. Gralnick, D. R. Bond, *Plos One* **2011**, *6*, e16649.

[26] E. Yeager, *J. Mol. Catal.* **1986**, *38*, 5.

[27] J. P. Collman, P. Denisevich, Y. Konai, M. Marrocco, C. Koval, F. C. Anson, *J. Am. Chem. Soc.* **1980**, *102*, 6027.